Optical Materials: X 26 (2025) 100407

Contents lists available at ScienceDirect

Optical Materials: X

journal homepage: www.journals.elsevier.com/optical-materials-x

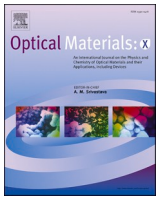

$CsPbCl_3:Yb^{3+}$ nanocrystals: Adverse effects of colloidally stable ytterbium-rich reaction by-products on luminescent down-conversion performance

Mathis Van de Voorde [a,b,*], Damien Hudry [b], Dmitry Busko [b], Bryce S. Richards [b,c], Rebecca Saive [a]

[a] University of Twente, Enschede, 7522NB, the Netherlands
[b] Institute of Microstructure Technology, Karlsruhe Institute of Technology, Karlsruhe, Germany
[c] Light Technology Institute, Karlsruhe Institute of Technology, Karlsruhe, Germany

ARTICLE INFO

Keywords:
Quantum-cutting
Down-conversion
Lead halide perovskite nanocrystals
Near infra-red emission
Energy transfer
Lanthanides

ABSTRACT

The development of near infra-red (NIR) emitting down-converters is a promising route for improving photovoltaic output through efficient light management. Quantum-cutting Yb^{3+}-doped $CsPbCl_3$ nanocrystals (NCs) are interesting for this application due to their high photoluminescence quantum yields (PLQY >100 %) and attractive NIR spectral properties which include high absorption cross section and minimal overlap between absorption and emission spectra. In this work, we fabricated $CsPbCl_3:Yb^{3+}$ NCs with the hot-injection method and studied them using structural/optical characterization methods such as x-ray diffraction, scanning transmission electron microscopy, energy-dispersive x-ray spectroscopy, fluorescence lifetime and quantum yield measurements. We found that the hot-injection method is susceptible to the formation of colloidally stable Yb-rich reaction by-products. After separating these by-products from the NCs, NIR PLQY increased by a relative 46 %. Although the PLQY values recorded in this study are 4–7 times lower than in other studies, these findings may explain some discrepancies in photoluminescence efficiency reported with this material.

1. Introduction

Cutting-edge luminescent materials have found their use in many applications such as displays [1], bio-imaging [2,3] and photovoltaics (PV) [4,5]. A particularly appealing physical effect that can enhance performance beyond ordinary down-shifting is quantum cutting, also known as down-conversion (DC), which results in the emission of two low-energy NIR photons following the absorption of a single high-energy ultraviolet (UV)/blue photon. DC luminophores could boost the performance of today's PV technologies in the following ways: i) placing a DC layer on top of a silicon (Si) solar cell to enhance its short-wavelength external quantum efficiency (EQE); and ii) using the DC material as a luminophore in a luminescent solar concentrator (LSC) [6]. Although DC has long been a holy grail for luminescent materials in PV applications [7], many materials investigated until now fell short in one or more areas, most typically a poor absorption cross-section, which resulted in the >190 % *internal* PLQY (per *absorbed* photon) values resulting in only 30 % *external* PLQY (per *incident* photon) [8].

In recent years, a novel class of luminophores has been considered for down-shifting/down-converting applications: lead halide perovskite nanocrystals (NCs). In 2015, Protesescu et al. successfully synthesized near-unity quantum yield $CsPbX_3$ (X = Cl, Br, I) perovskite NCs using the hot-injection method [9]. Since then, extensive research [10–13] has focused on the optimization and exploration of synthetic conditions for reliable achievement of highly efficient perovskite emitters. It is worth noting that the powder analogs of these NCs are also being investigated for their intriguing structural/optical properties [14–17]. The perovskite NCs offer benefits such as large absorption cross-sections and narrow emission bands [18], which makes them promising candidates for LSC applications. However, challenges arise from their limited optical and chemical stability [19,20] as well as their significant spectral overlap between absorption and emission profiles (in other words a small Stokes shift or, conversely, a high overlap integral [21]), which is known to be the main performance-killer in any LSC of reasonable size [22]. This overlap raises the likelihood of reabsorption events, which subsequently leads to losses due to suffering multiple: i) sub-unity

* Corresponding author. University of Twente, Enschede, 7522NB, the Netherlands.
E-mail address: m.a.n.vandevoorde@utwente.nl (M. Van de Voorde).

https://doi.org/10.1016/j.omx.2025.100407
Received 7 November 2024; Received in revised form 18 February 2025; Accepted 19 February 2025
Available online 22 February 2025

photoluminescence quantum yield (PLQY) events; and ii) isotropic re-emissions of photons which can exit via the LSC's escape cone [23]. To tackle this issue, researchers have investigated the introduction of dopants in the perovskite matrix to achieve exciton energy transfer from the semiconductor to a luminescent ion. Pan et al. [24] established that cations from the trivalent lanthanide (Ln^{3+}) series were able to enter the host matrix structure by replacing Pb^{2+} ions inside the corner-sharing halide octahedra. However, their experiments indicated a rather unsuccessful energy transfer from the perovskite to Ln^{3+} ions with only one remarkable exception. Interestingly, the authors showed that $CsPbCl_3$ NCs doped with Yb^{3+} exhibited significant near-infrared (NIR) photoluminescence compared to other Ln^{3+} dopant ions, which was attributed to an efficient DC.

The DC mechanism proposed by Milstein et al. [25]. states that with the assistance of a shallow trap state (Pb^{2+} vacancy induced by the aliovalent incorporation of Yb^{3+} in the matrix), the exciton energy is transferred to two neighboring Yb^{3+} ions, thereby exciting two low energy Yb^{3+} states ($^2F_{5/2}$) that eventually relax to the ground state ($^2F_{7/2}$) to emit a total of two photons at ~990 nm. A schematic illustration of this mechanism is shown in Fig. 1. PLQY values that exceed 100 % have been reported by several research groups with NCs of this material [24,26–28]. Interestingly, a broad range of NIR PLQY values (110–170 %) were recorded with samples that originated from similar reaction conditions [25,26,28,29], as summarized in a recent review by Timkina et al. [30].

To elucidate the origin of these discrepancies, we have synthesized both Yb^{3+}-doped and undoped $CsPbCl_3$ NCs under the same conditions as used in the reaction yielding the variable PLQYs [25] (summarized in Table S1). We demonstrate how an unwanted formation of colloidally-stable reaction by-products (RBPs) negatively influences the optical properties of the NCs. Both phases (i.e., nanocrystals and RBPs) were successfully separated after the complete sedimentation of the by-product approximately one month after the synthesis. The colloidal solution is analyzed before and after RBP removal by scanning transmission electron microscopy (STEM), x-ray diffraction (XRD), energy-dispersive x-ray (EDX) spectroscopy from STEM images, as well as time-resolved photoluminescence (TRPL) spectroscopy and absolute PLQY measurements. Although the absolute PLQY values recorded in this work (~24.3 %) are 4 – 7-times lower than those previously reported with this material, we believe the undetected presence of such by-products in synthesized samples could explain certain inconsistencies in PLQY values reported in the literature.

2. Results & discussion

2.1. Nanocrystal synthesis

To synthesize the NCs, we first dissolved metal-oleate precursors in octadecene, oleylamine and oleic acid inside a 3-neck flask under inert conditions (Fig. S1). Then, we swiftly injected trimethylsilyl chloride in the reactor which was heated at 240 °C to achieve a rapid burst of nucleation/growth of the NCs. The reaction was quenched after a few seconds by placing the reactor in an ice bath and the resulting nanocrystals were carefully extracted (Fig. S2) through washing and purification steps (full protocols available in the Supplementary Information A. Methods, together with additional lower magnification STEM images (Fig. S3)).

2.2. Structure, morphology and composition of nanocrystals/RBPs

The STEM images in Fig. 2 depict the morphology of the synthesized Yb^{3+}-doped/undoped $CsPbCl_3$ NCs. Fig. 2a shows the morphology of the undoped $CsPbCl_3$ NC sample. Here, a single fraction of monodisperse nanocubes can be observed. Conversely, in Fig. 2b, we note the presence of an additional phase together with the Yb^{3+}-doped nanocubes. This additional phase is distinguishable from the monodisperse nanocubes due to the darker appearance (indicative of a heavier element or higher concentration of it), spherical shapes and larger sizes of the particles. Approximately one month after the synthesis of the doped sample, a sediment was observed at the bottom of the stored vial. The sediment was removed by centrifugation and the remaining colloidal suspension was kept for further analysis. Fig. 2c shows a STEM image of the colloidal suspension after the removal of the sediment. This image clearly shows that the RBPs were extracted during the centrifugation step, leaving behind a monodisperse fraction of nanocubes. The complete removal of the RBPs is also shown quantitatively in the particle size distribution histograms plotted in Fig. 2d. XRD patterns in the following section confirm these particles are in fact a by-product of the reaction.

The three XRD patterns shown in Fig. 3 were recorded from the same samples imaged in Fig. 2, namely the undoped $CsPbCl_3$ and the Yb^{3+}-doped $CsPbCl_3$ with and without RBPs. The presence of the cubic perovskite phase is evident in these plots for both the doped (blue and green curves) and undoped (red curve) samples. The diffraction peaks were indexed with the cubic-phase $CsPbCl_3$ reference card (ICSD 98-002-3108). The absence of the (110) and the (112) planes (22.42° and 39.35°, respectively) in the blue curve can be attributed to the dilution step this sample went through for RBP extraction (see Supplementary

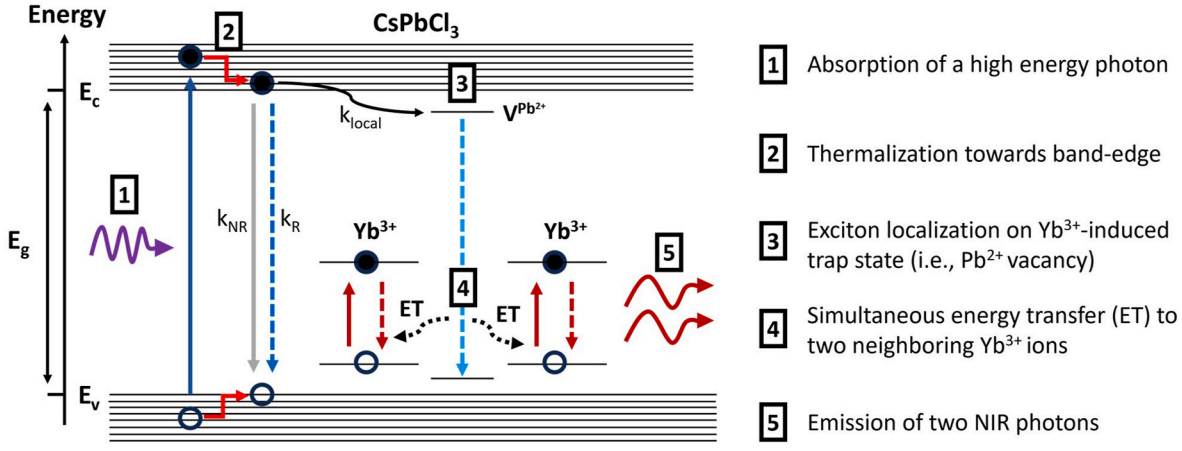

Fig. 1. Schematic illustration of the DC process in $CsPbCl_3$:Yb^{3+}. The mechanism is divided here in five steps: 1) The absorption of a high energy photon by the $CsPbCl_3$ matrix. 2) Thermalization of the exciton towards the band-edge. Here, 3 competitive processes occur: radiative and non-radiative recombination of the exciton (k_R and k_{NR}) as well as the localization of the exciton in the Pb^{2+} vacancy-induced energy landscape distortion (k_{local}, step 3). 4) Simultaneous energy transfer towards two neighboring Yb^{3+} ions. 5) Emission of two NIR photons.

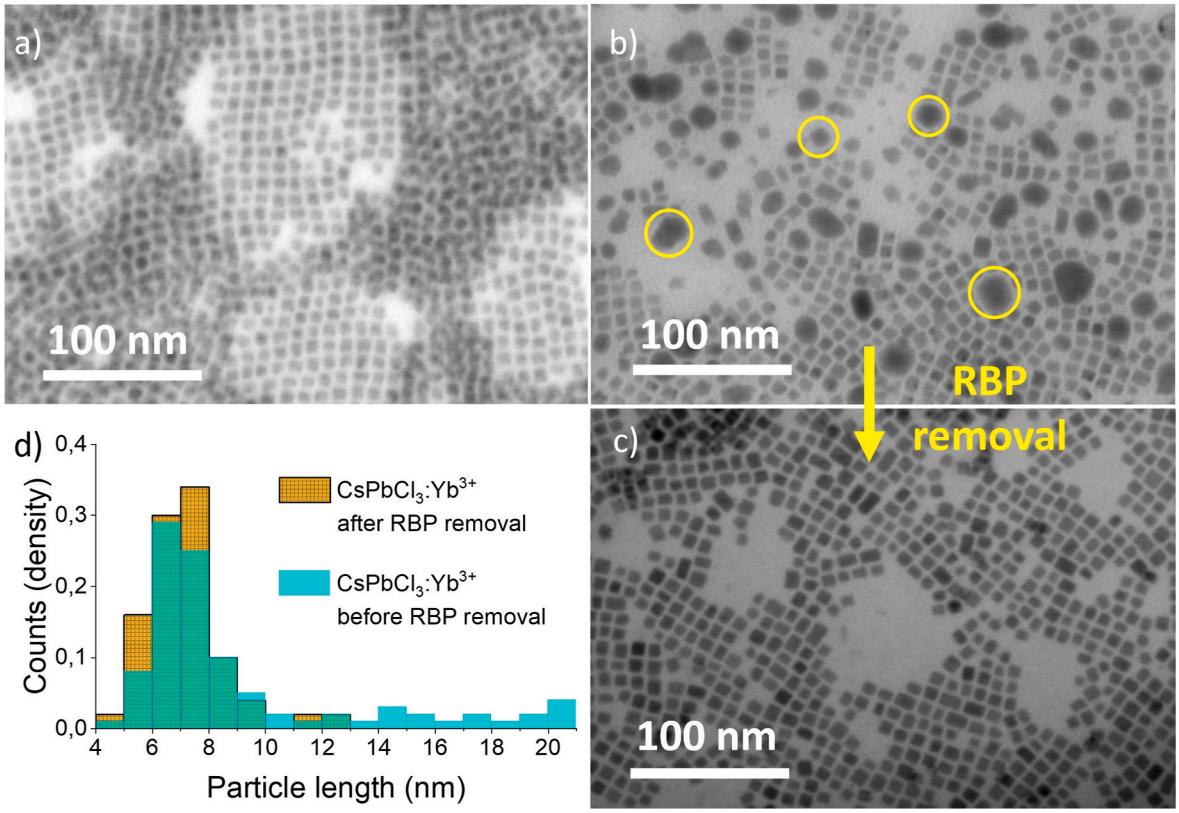

Fig. 2. STEM images of a) undoped $CsPbCl_3$ NCs. b) $CsPbCl_3$:Yb^{3+} NCs before separation from the Yb^{3+}-rich RBPs, where some characteristic particles are highlighted by a yellow circle. c) $CsPbCl_3$:Yb^{3+} NCs after removal of the Yb^{3+}-rich RBPs. d) Overlaid size distributions of b) (cyan) and c) (patterned brown).

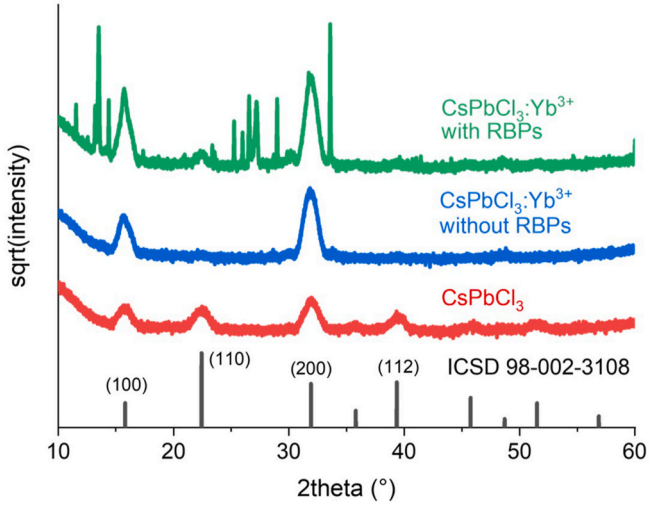

Fig. 3. XRD spectra of drop-casted $CsPbCl_3$ NCs (red), $CsPbCl_3$:Yb^{3+} without Yb-rich RBPs (blue) and $CsPbCl_3$:Yb^{3+} with Yb^{3+}-rich RBPs (green). ICSD 98-002-3108 (black) showing the cubic-phase $CsPbCl_3$ reference card. To improve clarity, the y-axis plots the square root of the measured intensity.

Information A. Methods). Such a dilution could facilitate the formation of a well-ordered, preferentially oriented monolayer of nanocubes during drop-casting of the solution for analysis. Notably, additional peaks that confirm the presence of multiple phases are observed in the pattern obtained with the doped sample prior to centrifugation (green curve). In all three samples, the (100) and (200) planes, at 15.80° and 31.91° respectively, are present in the diffraction patterns. It is important to mention, that the structural nature of the RBPs shown in the green XRD pattern is currently unknown as thorough screening through standard databases such as the ICCD PDF (HighScore [31] and WinXpow programs) yielded no conclusive results.

To shed light on the elemental nature of the RBPs, EDX measurements were conducted on the sample which contains both the cubic NCs and spherical particles (see Fig. 2b). Fig. 4a is the STEM image of the sample before the EDX measurement. In this image we can single out the RBP, which has a large spherical shape, from the smaller nanocubes. From the elemental map in Fig. 4c, an enrichment in Yb counts is visible in the area where the RBP lies, while the maps in Fig. 4d–f showcase a spread distribution of the Cs, Pb and Cl signal. From this we can conclude the RBP phase is Yb^{3+}-rich. On the areas with only the cubic NCs, we observe a weaker Yb signal as compared to the Yb signal obtained from the RBP. This indicates the presence of low concentration of Yb^{3+} either within the NCs or on their surface. More elemental maps strengthening this claim are available in the Supplementary Information (Figs. S4 and 5).

The observed secondary phase in Fig. 2b, now identified as Yb^{3+}-rich, can likely be attributed to the large quantity of $Yb(CH_3COO)_3$ used in the synthesis. According to ICP-AES measurements by Milstein *et. al.* [25], less than 10 % of the introduced dopant enters the crystalline structure in the used reaction conditions. Consequently, a considerable amount of precursor is available to form by-products like the ones observed in Fig. 2b. Moreover, the complete sedimentation of RBPs, which led to the successful separation of the two phases, is believed to be due to the lack of ligands stabilizing the surface of the spherical particles. While the $CsPbCl_3$ NCs profit from steric stabilization, the RBPs tend to aggregate over time. These heavier aggregates then deposit as a sediment on the bottom of the vial at a faster pace than the NCs. This process could be sped up by prolonged centrifugation steps after the synthesis. In the following section, optical measurements (i.e., absorbance/emission/excitation spectra, lifetime and PLQY) are shown to demonstrate to what extent the RBPs impact the performance of the

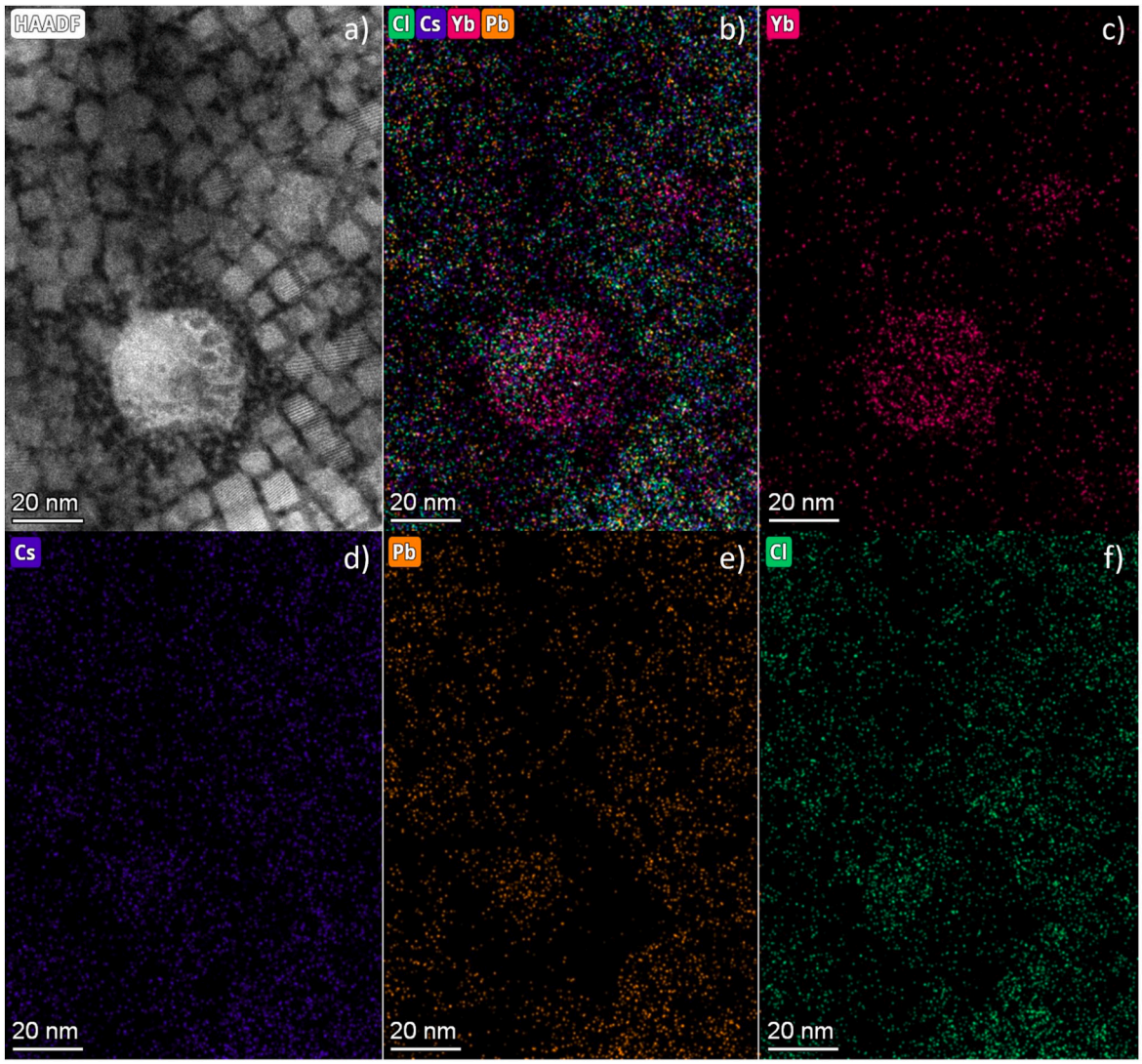

Fig. 4. EDX elemental maps of $CsPbCl_3$:Yb^{3+} nanocrystals with Yb^{3+}-rich RBPs. a) STEM image of sample before EDX scan, b) Atomic distribution color map, c)-f) Single element maps of Yb, Cs, Pb and Cl, respectively.

doped sample.

2.3. Host-dopant energy transfer characterization

Normalized absorption and photoluminescence spectra are plotted in Fig. 5a. A pronounced Stokes shift is apparent in the doped sample (black) as compared to the undoped sample (blue). Evidently, the doped sample emits light from the Yb^{3+} energy level ($^2F_{5/2} \rightarrow {}^2F_{7/2}$ transition, emission peak at ~990 nm), while absorbing at the host-matrix band edge (~405 nm). Note, that the doped sample also exhibits blue emission from the host matrix. This band-edge emission overlaps almost perfectly with the one from the undoped sample. For further information on excitonic emission lifetimes and PLQY of both doped and undoped samples, please refer to the Supplementary Information (Fig. S6 & comments). From the photoluminescence excitation (PLE) spectrum shown in Fig. 5b, we can deduce that the doped sample only emits in the NIR when excited with photons of energies higher than the $CsPbCl_3$ band gap. This is visible by the abrupt drop in NIR peak intensity when the excitation wavelength is increased above 405 nm. The NIR lifetimes, as presented in Fig. 5c, resulted in a significant increase (from 1.1 to 1.8 ms – values obtained when fitting both lifetimes with single component decay functions) after the removal of the RBPs. The sample without RBPs was fitted with a single-component exponential decay function (**Eq. S(1)**). The lifetime extracted from that first fit (τ_0, **Eq. S(1)**) was used as an input for the double-component exponential decay fit (τ_2, **Eq. S(2)**) of the sample with RBPs in order to excavate the lifetime of the impurities. As expected, a much shorter lifetime (τ_1, **Eq. S(2)**) is extracted, likely caused by the increased Yb^{3+} concentration in the RBPs that enhances energy migration and results in a pronounced parasitic cross-relaxation. To quantify this, absolute PLQY measurements are performed exciting the NCs using a 405 nm laser.

It is known, that efficiency of down-conversion in such materials depends on an excitation intensity [26]. To probe a larger range of excitation intensities, two separate PLQY measurements were carried out on the samples: a high-power and a low-power density measurement. The high-power density measurement was performed with a direct hit of the laser on the sample while the low-power density measurement was done with the laser hitting the integrating sphere wall first. Equations and further explanation of these two measurements are available in the Supplementary Information, section A. Methods. The absolute NIR PLQY results for both clean material and the one with RBPs are plotted in Fig. 5d, where the x-axis represents the excitation power density and the y-axis the measured absolute NIR quantum yield. We observe that the sample demonstrates an effective increase in performance upon RBP removal (from 16.7 to 24.3 % absolute NIR PLQY at low excitation power densities) which is consistent with the longer

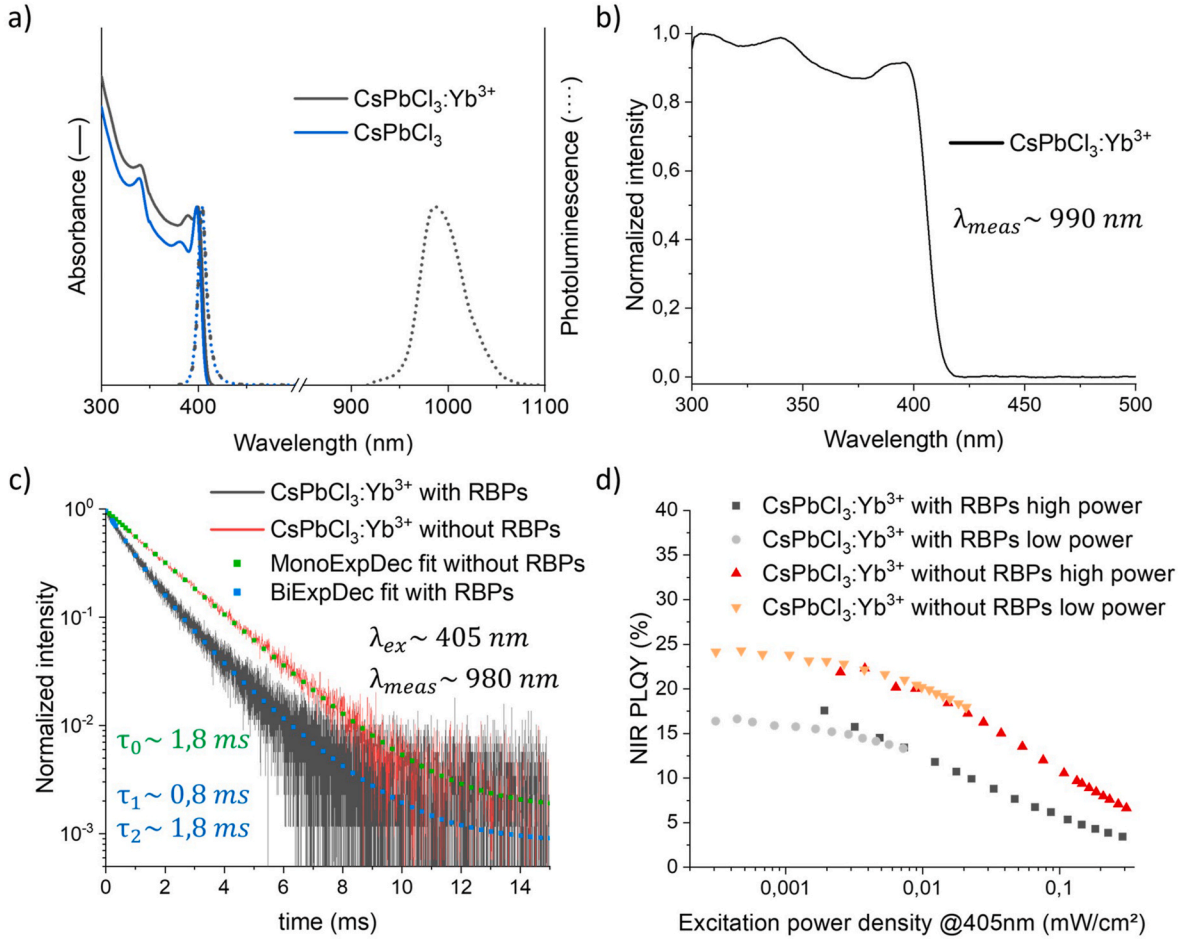

Fig. 5. a) Normalized absorption (full line) and emission (dotted line) of $CsPbCl_3$ (blue) and $CsPbCl_3$:Yb^{3+} with RBPs (black). b) PLE spectrum of $CsPbCl_3$:Yb^{3+} probed at 990 nm. c) Yb^{3+} emission lifetime for the $CsPbCl_3$:Yb^{3+} sample with (black) and without (red) Yb^{3+}-rich RBPs and their exponential decay fits (blue and green squares, respectively), excited at 405 nm and probed at 980 nm. d) NIR absolute PLQY at high and low excitation power density of the $CsPbCl_3$:Yb^{3+} sample with (black squares and grey circles, respectively) and without (red up-facing and orange down-facing triangles, respectively) Yb^{3+}-rich RBPs.

measured lifetime. It is evident that for both samples, before and after RBP removal, the PLQY decreases when the excitation power density is increased. This is consistent with previous reports from Erickson et al. [26] that attribute the power density dependence to Auger-type cross--relaxation processes caused by the exciton energy transfer from the Pb^{2+}-vacancy trap state to an already excited $^2F_{5/2}$ Yb^{3+} energy level. The authors proposed a kinetic model describing two different non-radiative Auger cross-relaxation processes that occurred at rates competitive with the DC process. These cross-relaxation processes become more pronounced at higher excitation power densities due to the population buildup of the $^2F_{5/2}$ states, which in turn leads to photoluminescence saturation.

2.4. Author comments & recommendations

From an experimental perspective, the hot-injection synthetic pathway for producing lead halide perovskites exhibits certain limitations. Although many groups have been able to successfully synthesize high-quality perovskite NCs via the hot-injection method, the use of precursors in non-stoichiometric proportions introduces complexities in the effective control of reaction outcomes. This is especially important within the context of a considerably dynamic environment (i.e., inhomogeneous reactor temperature, swift precursor injection and fast reaction kinetics). Consequently, the hot-injection synthesis outcome is highly dependent/sensitive to the reaction environment which involves the chemicals used, the apparatus quality, the moisture content, as well as human-related factors. Therefore, the effective control of doping reactions in PNC matrices presents itself as a challenge with the introduction of an additional layer of complexity (i.e., the dopant). During the synthesis of $CsPbCl_3$:Yb^{3+}, the use of dopant in alloy-like quantities (0.8:1 ratio of Yb^{3+}:Pb^{2+}) only ever results in a marginal fraction of dopant incorporation in the matrix [25]. As a result, the unreacted material is available to form unwanted by-products with other unreacted precursors. This study demonstrates that such derivate phases can remain colloidally stable for a certain amount of time and exert an adverse effect on the sample performance. We note, that such secondary phases are usually eliminated through washing/purifications steps. Yet, if impurities remain present even after those steps (i.e., the ones shown in this work), more advanced purification methods and optimization of the nanocrystal extraction process can be performed [32–35].

With this in mind, we would like to emphasize that there is much to gain from improving the replicability of the synthetic procedures. One effective way of doing so is by providing more extensive descriptions of the synthetic procedures and characterization methods: That includes additional information on the drying process of the precursors (e.g., pressure values of vacuum cycles), on the precursor dissolution step (e.g., precise step times, temperatures, pressure values and issues encountered in trials), as well as additional insights into the extraction process (including characteristics such as pellet color, relative centrifugal forces expressed in acceleration force (xg) instead of revolutions per minute (RPM), and visual documentation of the raw and extracted product).

3. Conclusion

In this work, cubic-phase $CsPbCl_3$ NCs doped with Yb^{3+} were synthesized through the hot-injection technique. NIR emission upon UV excitation was successfully achieved, however with PLQY values 4–7 times lower than what has been reported in literature with this material. A secondary phase that likely results from the use of alloy-like quantities of dopants during the synthesis was found to substantially impact the optical efficiency of the overall sample. Undetected, such by-products could potentially account for discrepancies in measured down-conversion efficiencies. We argue the current hot-injection method is suboptimal for the investigation of RE^{3+}-doping reactions in halide perovskite NCs due to the evidently difficult integration of the dopant in the matrix as well as the lack of control in this highly dynamic reaction environment. Future research aimed at improving the incorporation of Yb^{3+} in the perovskite matrix with meticulously described reaction/measurement conditions is therefore essential to reliably achieve highly efficient down-converting perovskite nanocrystals.

CRediT authorship contribution statement

Mathis Van de Voorde: Writing – review & editing, Writing – original draft, Visualization, Methodology, Investigation, Formal analysis, Data curation. **Damien Hudry:** Writing – review & editing, Validation, Supervision, Resources, Methodology. **Dmitry Busko:** Writing – review & editing, Validation, Supervision, Resources, Methodology. **Bryce S. Richards:** Writing – review & editing, Validation, Supervision, Resources, Conceptualization. **Rebecca Saive:** Writing – review & editing, Validation, Supervision, Project administration, Funding acquisition, Data curation, Conceptualization.

Data statement

Data will be made available on request.

Declaration of competing interest

The authors declare that they have no known competing financial interests or personal relationships that could have appeared to influence the work reported in this paper.

Acknowledgments

The UT team gratefully acknowledge the Dutch Research Council (NWO) for funding this research through the Knowledge and Innovation Covenant (KIC) program. This publication is part of the project Diffuse Irradiance Redirector for Efficient ConcenTration (DIRECT) (with project number KICH1.ED02.20.006 of the research programme NWO Kennis-en innovatieconvenant Innovations for Wind and Solar which is (partly) financed by the Dutch Research Council (NWO). The KIT team gratefully acknowledge the financial support provided by the Helmholtz Association: (i) a Recruitment Initiative Fellowship for B.S.R.; (ii) the funding of chemical synthesis equipment from the Helmholtz Materials Energy Foundry (HEMF); and (iii) Research Field Energy – Program Materials and Technologies for the Energy Transition – Topic 1 Photovoltaics. We acknowledge the following researchers for their contributions to this work. Dr. Melissa Goodwin and dr. Martina Tsvetanova from the MESA + institute at UT for performing the STEM and EDX measurements and fitting the obtained spectra. Dr. Eduard Madirov at IMT (KIT) for assisting with optical characterization and performing Yb^{3+} emission lifetime measurements. Dr. Ian Howard at IMT (KIT) for advising in meetings. Vadim Ratovskii for assisting with the phase identification of the impurities. Members of the Saive group at the IMS group (UT) for continuous input during group meetings.

Appendix A. Supplementary data

Supplementary data to this article can be found online at https://doi.org/10.1016/j.omx.2025.100407.

Data availability

Data will be made available on request.

References

[1] M.A. Triana, E.L. Hsiang, C. Zhang, Y. Dong, S.T. Wu, Luminescent nanomaterials for energy-efficient display and Healthcare, ACS Energy Lett. 7 (3) (2022) 1001–1020, https://doi.org/10.1021/acsenergylett.1c02745.
[2] W. Liang, S. He, S. Wu, Fluorescence imaging in second near-infrared window: developments, challenges, and opportunities, Adv Nanobiomed Res 2 (11) (2022) 2200087, https://doi.org/10.1002/anbr.202200087.
[3] F. Arteaga Cardona, N. Jain, R. Popescu, et al., Preventing cation intermixing enables 50% quantum yield in sub-15 nm short-wave infrared-emitting rare-earth based core-shell nanocrystals, Nat. Commun. 14 (1) (2023), https://doi.org/10.1038/s41467-023-40031-4.
[4] S.M. Ferro, M. Wobben, B. Ehrler, Rare-earth quantum cutting in metal halide perovskites-a review, Mater. Horiz. 8 (4) (2021) 1072–1083, https://doi.org/10.1039/d0mh01470b.
[5] B.S. Richards, D. Hudry, D. Busko, A. Turshatov, I.A. Howard, Photon upconversion for photovoltaics and photocatalysis: a critical review, Chem Rev 121 (15) (2021) 9165–9195, https://doi.org/10.1021/acs.chemrev.1c00034.
[6] X. Luo, T. Ding, X. Liu, Y. Liu, K. Wu, Quantum-cutting luminescent solar concentrators using ytterbium-doped perovskite nanocrystals, Nano Lett. 19 (1) (2019) 338–341, https://doi.org/10.1021/acs.nanolett.8b03966.
[7] B.S. Richards, Luminescent layers for enhanced silicon solar cell performance: down-conversion, Sol. Energy Mater. Sol. Cell. 90 (9) (2006) 1189–1207, https://doi.org/10.1016/j.solmat.2005.07.001.
[8] C. Feldmann, T.J. Jüstel, C.R. Ronda, D.U. Wiechert, Quantum Efficiency of Down-Conversion Phosphor LiGdF 4 : *Eu*, vol. 92, 2001.
[9] L. Protesescu, S. Yakunin, M.I. Bodnarchuk, et al., Nanocrystals of cesium lead halide perovskites (CsPbX3, X = Cl, Br, and I): novel optoelectronic materials showing bright emission with wide color gamut, Nano Lett. 15 (6) (2015) 3692–3696, https://doi.org/10.1021/nl5048779.
[10] K. Vighnesh, S. Wang, H. Liu, A.L. Rogach, Hot-injection synthesis protocol for green-emitting cesium lead bromide perovskite nanocrystals, ACS Nano 16 (12) (2022) 19618–19625, https://doi.org/10.1021/acsnano.2c11689.
[11] G. Li, J. Huang, H. Zhu, Y. Li, J.X. Tang, Y. Jiang, Surface ligand engineering for near-unity quantum yield inorganic halide perovskite QDs and high-performance QLEDs, Chem. Mater. 30 (17) (2018) 6099–6107, https://doi.org/10.1021/acs.chemmater.8b02544.
[12] G. Almeida, O.J. Ashton, L. Goldoni, et al., The phosphine oxide route toward lead halide perovskite nanocrystals, J. Am. Chem. Soc. 140 (44) (2018) 14878–14886, https://doi.org/10.1021/jacs.8b08978.
[13] M. Imran, V. Caligiuri, M. Wang, et al., Benzoyl halides as alternative precursors for the colloidal synthesis of lead-based halide perovskite nanocrystals, J. Am. Chem. Soc. 140 (7) (2018) 2656–2664, https://doi.org/10.1021/jacs.7b13477.
[14] C.A. López, C. Abia, M.C. Alvarez-Galván, et al., Crystal structure features of CsPbBr3 perovskite prepared by mechanochemical synthesis, ACS Omega 5 (11) (2020) 5931–5938, https://doi.org/10.1021/acsomega.9b04248.
[15] K.A. Dagnall, A.M. Conley, L.U. Yoon, H.S. Rajeev, S.H. Lee, J.J. Choi, Ytterbium-doped cesium lead chloride perovskite as an X-ray scintillator with high light yield, ACS Omega 7 (24) (2022) 20968–20974, https://doi.org/10.1021/acsomega.2c01712.
[16] M. Stefanski, M. Ptak, A. Sieradzki, W. Strek, Optical characterization of Yb3+: CsPbCl3 perovskite powder, Chem. Eng. J. 408 (2021), https://doi.org/10.1016/j.cej.2020.127347.
[17] L. Piveteau, M. Aebli, N. Yazdani, et al., Bulk and nanocrystalline cesium lead-halide perovskites as seen by halide magnetic resonance, ACS Cent. Sci. 6 (7) (2020) 1138–1149, https://doi.org/10.1021/acscentsci.0c00587.
[18] G. Nedelcu, L. Protesescu, S. Yakunin, M.I. Bodnarchuk, M.J. Grotevent, M. V. Kovalenko, Fast anion-exchange in highly luminescent nanocrystals of cesium lead halide perovskites (CsPbX3, X = Cl, Br, I), Nano Lett. 15 (8) (2015) 5635–5640, https://doi.org/10.1021/acs.nanolett.5b02404.
[19] B.W. Boote, H.P. Andaraarachchi, B.A. Rosales, et al., Unveiling the photo- and thermal-stability of cesium lead halide perovskite nanocrystals, ChemPhysChem 20 (20) (2019) 2647–2656, https://doi.org/10.1002/cphc.201900432.
[20] H. Huang, M.I. Bodnarchuk, S.V. Kershaw, M.V. Kovalenko, A.L. Rogach, Lead halide perovskite nanocrystals in the research spotlight: stability and defect tolerance, ACS Energy Lett. 2 (9) (2017) 2071–2083, https://doi.org/10.1021/acsenergylett.7b00547.
[21] C. Yang, M. Moemeni, M. Bates, W. Sheng, B. Borhan, R.R. Lunt, High-performance near-infrared harvesting transparent luminescent solar concentrators, Adv. Opt. Mater. 8 (8) (2020), https://doi.org/10.1002/adom.201901536.
[22] B.S. Richards, I.A. Howard, Luminescent solar concentrators for building integrated photovoltaics: opportunities and challenges, Energy Environ. Sci. (2023), https://doi.org/10.1039/d3ee00331k. Published online July 7.

[23] C. Tummeltshammer, A. Taylor, A.J. Kenyon, I. Papakonstantinou, Losses in luminescent solar concentrators unveiled, Sol. Energy Mater. Sol. Cell. 144 (2016) 40–47, https://doi.org/10.1016/j.solmat.2015.08.008.
[24] G. Pan, X. Bai, D. Yang, et al., Doping lanthanide into perovskite nanocrystals: highly improved and expanded optical properties, Nano Lett. 17 (12) (2017) 8005–8011, https://doi.org/10.1021/acs.nanolett.7b04575.
[25] T.J. Milstein, D.M. Kroupa, D.R. Gamelin, Picosecond quantum cutting generates photoluminescence quantum yields over 100% in ytterbium-doped CsPbCl3 nanocrystals, Nano Lett. 18 (6) (2018) 3792–3799, https://doi.org/10.1021/acs.nanolett.8b01066.
[26] C.S. Erickson, M.J. Crane, T.J. Milstein, D.R. Gamelin, Photoluminescence saturation in quantum-cutting Yb3+-doped CsPb(Cl1- xBrx)3 perovskite nanocrystals: implications for solar downconversion, J. Phys. Chem. C 123 (19) (2019) 12474–12484, https://doi.org/10.1021/acs.jpcc.9b01296.
[27] X. Shen, Z. Wang, C. Tang, et al., Near-infrared LEDs based on quantum cutting-activated electroluminescence of ytterbium ions, Nano Lett. 23 (1) (2023) 82–90, https://doi.org/10.1021/acs.nanolett.2c03679.
[28] H. Huang, R. Li, S. Jin, et al., Ytterbium-doped CsPbCl3Quantum cutters for near-infrared light-emitting diodes, ACS Appl. Mater. Interfaces 13 (29) (2021) 34561–34571, https://doi.org/10.1021/acsami.1c09421.
[29] T.J. Milstein, K.T. Kluherz, D.M. Kroupa, C.S. Erickson, J.J. De Yoreo, D. R. Gamelin, Anion exchange and the quantum-cutting energy threshold in ytterbium-doped CsPb(Cl 1- x Br x) 3 perovskite nanocrystals, Nano Lett. 19 (3) (2019) 1931–1937, https://doi.org/10.1021/acs.nanolett.8b05104.
[30] Y.A. Timkina, V.S. Tuchin, A.P. Litvin, E.V. Ushakova, A.L. Rogach, Ytterbium-doped lead–halide perovskite nanocrystals: synthesis, near-infrared emission, and open-source machine learning model for prediction of optical properties, Nanomaterials 13 (4) (2023), https://doi.org/10.3390/nano13040744.
[31] The HighScore suite, T. Degen, M. Sadki, E. Bron, U. König, G. Nénert, Powder Diffraction/Volume 29/Supplement S2, December 2014, pp. S13–S18.
[32] Y. Zhang, T.D. Siegler, C.J. Thomas, et al., A “tips and tricks” practical guide to the synthesis of metal halide perovskite nanocrystals, Chem. Mater. 32 (13) (2020) 5410–5423, https://doi.org/10.1021/acs.chemmater.0c01735.
[33] M. De Franco, M. Cirignano, T. Cavattoni, H. Bahmani Jalali, M. Prato, F. Di Stasio, Facile purification protocol of CsPbBr3 nanocrystals for light-emitting diodes with improved performance, Opt. Mater. X 13 (2022), https://doi.org/10.1016/j.omx.2021.100124.
[34] K. Hoshi, T. Chiba, J. Sato, et al., Purification of perovskite quantum dots using low-dielectric-constant washing solvent “diglyme” for highly efficient light-emitting devices, ACS Appl. Mater. Interfaces 10 (29) (2018) 24607–24612, https://doi.org/10.1021/acsami.8b05954.
[35] S. Zhou, Rapid separation and purification of lead halide perovskite quantum dots through differential centrifugation in nonpolar solvent, RSC Adv. 11 (45) (2021) 28410–28419, https://doi.org/10.1039/d1ra04578d.